Heliyon 8 (2022) e10025

Contents lists available at ScienceDirect

Heliyon

journal homepage: www.cell.com/heliyon

Research article

The simulated cooling performance of a thin-film thermoelectric cooler with coupled-thermoelements connected in parallel

Tingzhen Ming [a,b], Sen Chen [a], Yonggao Yan [c], Tingrui Gong [d], Jianlong Wan [e], Yongjia Wu [a,*]

[a] School of Civil Engineering and Architecture, Wuhan University of Technology, Wuhan 430070, Hubei, China
[b] School of Architectural Engineering, Huanggang Normal University, No. 146 Xingang Second Road, Huanggang 438000, China
[c] State Key Laboratory of Advanced Technology for Materials Synthesis and Processing, Wuhan University of Technology, Wuhan 430070, Hubei, China
[d] Microsystem & Terahertz Research Center, China Academy of Engineering Physics, Chengdu 610200, Sichuan, China
[e] School of Energy and Power Engineering, Huazhong University of Science and Technology, Wuhan 430074, Hubei, China

HIGHLIGHTS

- A novel thin-film thermoelectric cooler with better reliability was demonstrated.
- The cooling performance of the new thin-film thermoelectric cooler is quantified.
- The new thin-film thermoelectric cooler is less sensitive to the local cracks.

ARTICLE INFO

Keywords:
Thin-film thermoelectric cooler
Coefficient of performance
Reliability

ABSTRACT

The thermoelements of the traditional thin-film thermoelectric cooler (TEC) are connected electrically in series, thus the performance of traditional thin-film TEC reduces sharply when there is something wrong with any thermoelement. On account of this deficiency, we proposed a novel thin-film TEC with a couple of thermoelements electrically connected in parallel and then electrically connected in series to the next couple of thermoelements. The performance and reliability of the novel thin-film TEC is compared with the traditional thin-film TEC. The maximum cooling capacity, the maximum cooling temperature, and the coefficient of performance of the novel and the traditional thin-film TEC are systematically studied and compared when 0, 2, and 4 thermoelements are disabled, respectively. The results show that the performance and reliability of the novel thin-film TEC are superior to that of the traditional thin-film TEC, while the optimal electric current of the novel thin-film TEC current is 2.14 times of that for the traditional thin-film TEC. This work is of great significance to improving the performance and reliability of thin-film thermoelectric devices consisting of dozens of small thermoelements.

1. Introduction

Thermoelectric cooler (TEC) is a solid-state heat pump which has attracted many researchers' attention since 1950s due to its unique features of no compressors and refrigerants, no vibration and noise, as well as easy to be controlled and integrated [1]. The TEC consists of pairs of p-type and n-type thermoelements that are connected electrically in series and thermally in parallel between two ceramic plates [2, 3]. When a direct electrical current flows across the TEC, the Peltier heat is generated at the interface between the connectors and thermoelements. As a result, a temperature difference is built between the two ends of the TEC.

The cooling performance of the TEC is evaluated by the three key indicators, the maximum cooling capacity ($Q_{c,max}$), the maximum cooling temperature (ΔT_{max}), and the coefficient of performance (COP) [4, 5, 6, 7]. A single-stage TEC can achieve a ΔT_{max} up to 70 °C, or can transfer $Q_{c,max}$ at an utmost rate of 125 W under the extreme conditions [8]. Harman, et al. [9] found that the TEC made by the PbSeTe-based quantum dot superlattice could create a cold-end temperature of -18.5 °C, 43.7 °C below the room temperature. Min and Rowe [10] improved theoretical model of a TEC, the result indicated that the COP decreased with a reduction in the thermoelement length, while the cooling capacity increased until reaching a maximum value. And they also found the COP

* Corresponding author.
E-mail address: yjwu2019@whut.edu.cn (Y. Wu).

https://doi.org/10.1016/j.heliyon.2022.e10025
Received 6 March 2022; Received in revised form 11 April 2022; Accepted 18 July 2022

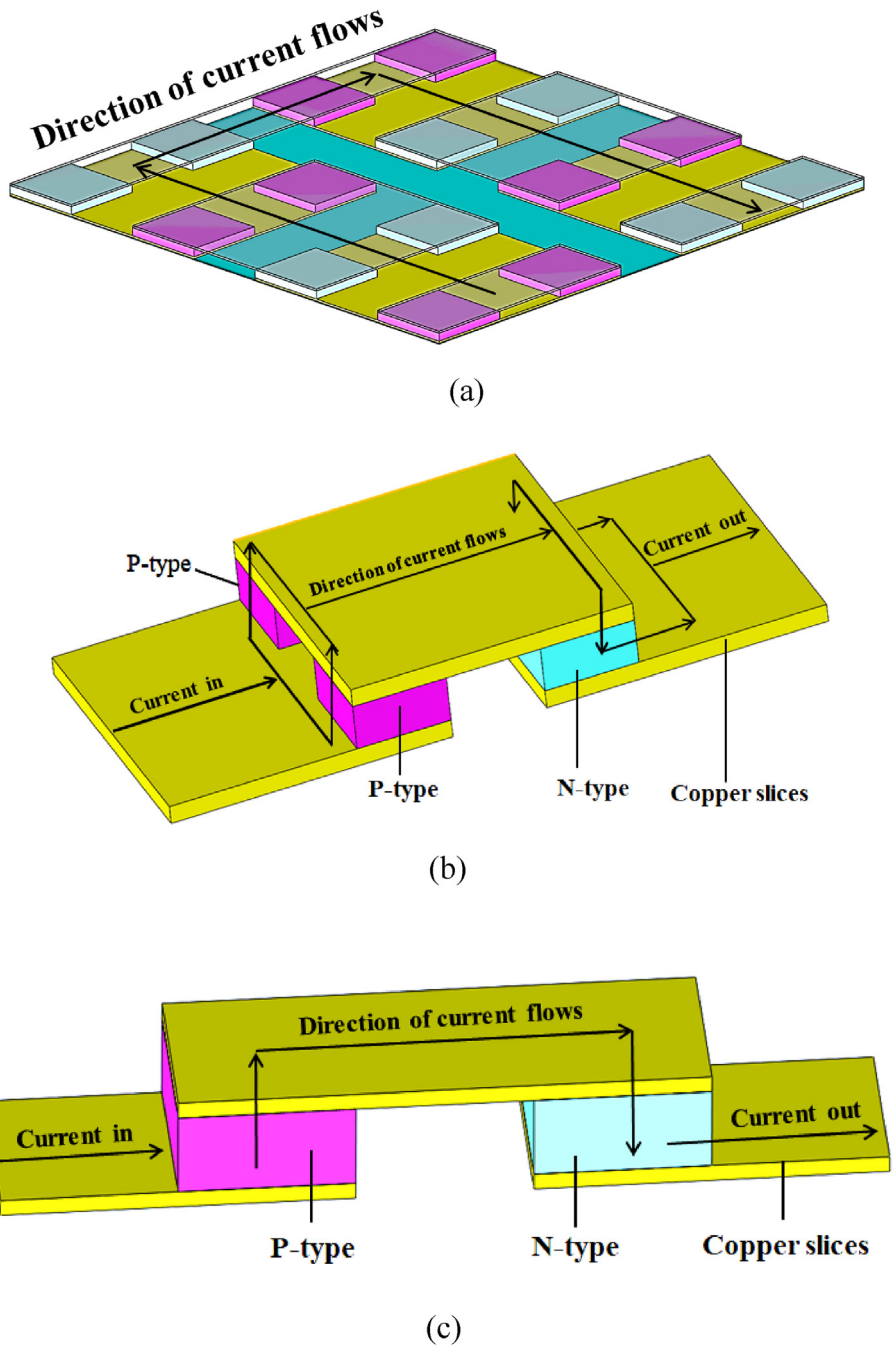

Figure 1. (a) Integral structure of the thin-film TEC; (b) the coupled-thermoelements of the thin-film TEC; (c) the local structure of the traditional thin-film TEC. ((a–c) are not drawn to scale.).

was 0.5–0.7 for a typical temperature difference of about 25–30 K. Lee and Kim [11] carried out numerical analysis to figure out the performance of the thermoelectric micro-cooler with the three-dimensional model, they found that the COP had the maximum value at a certain electrical current, and the COP increased with the decrease of temperature difference or the increase of the thermoelements thickness.

The performance of the TEC essentially depends on the figure of merit (ZT) of the thermoelectric materials. A higher ZT will lead to a better performance of the TEC [12]. Since the 1940s, tremendous efforts were devoted to increase the ZT of different materials [13]. If the ZT of the thermoelectric materials could be raised to 2 or 3, the TEC would be competitive with vapor compression cooling systems [8]. Unfortunately, bismuth telluride (Bi_2Te_3), being the best low-temperature thermoelectric (TE) material which was most widely employed in TEC, possesses a ZT value of about 1.0 [14]. The nano-structured thermoelectric materials, though owning a ZT higher than 2.0, were accused of being expensive and less stable than the bulk materials. So many researchers payed close attention to designing more efficient structure of the TEC using those existing TE materials to improve the cooling performance. Shen et al. [4] proposed the segmented TEC to enhance the cooling performance without increasing the overall figure of merit of the TE material. They investigated the segmented TEC by comparing it with the traditional thermoelectric coolers. The results showed that the $Q_{c,max}$ and ΔT_{max} of segmented thermoelectric element were larger than that of the traditional one. Gong et al. [15] performed three-dimensional numerical simulations to optimize design of a compact TEC using finite element method. The optimized TEC achieved the maximum cooling performance and high operation reliability. Nie et al. [16] designed a multi-stage

planar TEC, and performed a comprehensive numerical analysis focusing on the cooling performance of the multi-stage planar TEC. The results showed that the optimized multi-stage planar TEC could realize a ΔT_{max} of 8.2 K. Gross et al. [17] reported the design, fabrication, and testing of both one- and six-stage thin-film TECs, which achieved $\Delta T_{max} = 22.3$ K and $\Delta T_{max} = 17.9$ K, respectively.

With the rapid development of highly integrated and miniaturized micro-electronic devices, the generated power density increased sharply that it brought great challenges in the thermal management [18]. Thus, it is vital to provide high cooling flux to deal with this problem. Compared with the bulk TEC, the thin-film TEC with short thermoelement could significant enhance the cooling flux [8]. For example, the cooling flux of a bulk TEC is generally about 10 W/(cm^2) [19], while thin-film TEC has a cooling flux of more than 100 W/(cm^2) [20,21]. Thus, an increasing interest was focused on the thin-film TEC for its ultra-small size and excellent compatibility to cool ultra-high heat flux. Bulman et al. [22] demonstrated a external cooling of 55 K and an estimated heat pumping capacity of 128 W/cm^2 using the thin-film superlattice TEC. It was reported that electrical and thermal contact resistances increased significantly by the thermoelement shortening [23]. So, interfacial issues become increasingly prominent and non-negligible for the thin-film TEC [24]. In recent years, some researchers made many efforts in reducing the interfacial contact resistance. Chen [25] claimed that the thermal contact resistance was on the magnitude of 10^{-9}-10^{-8} $K{\cdot}m^2{\cdot}W^{-1}$ for a perfect interface based on the interfacial phonon transmission theory analysis. Yu et al. [26] acquired low contact resistivity of 10^{-7} $\Omega{\cdot}$cm^2 between Cu electrodes and Bi_2Te_3-based TE materials with ordered microstructures. There were still much room left for further reducing the thermal and electrical contact resistance.

The thin-film TEC was widely employed in thermal management of the highly integrated and miniaturized micro-electronic devices [27]. The thin-film TECs were required to have an operating life matching the life-cycle of the electronic devices, which usually ranged from several months to tens of years [28]. However, the electrical devices generated a high heat flux which created a harsh environment for the thin-film TECs. The large temperature gradients and thermal stresses [16] could results in the failure of the thin-film TEC and this issue should be carefully solved [15, 29, 30]. Some researchers demonstrated ring-shaped thermoelectric modules [31, 32], which showed significant superiority in the performance and reliability. However, considering dozens of thermoelements were electrically connected in series in the traditional TEC, any local crack could result in device level damage. To address this issue, we demonstrated a novel thin-film TEC with a couple of thermoelements electrically connected in parallel and then electrically connected in series to the next couple of thermoelements. It was noteworthy that the coupled thermoelements must be made of one kind of n-type or p-type semiconductor material consistently.

In this paper, we built a three-dimensional numerical model to investigate the cooling performance of the thin-film TEC, which considered the temperature dependent material properties. The maximum cooling capacity ($Q_{c,max}$), maximum cooling temperature (ΔT_{max}), and the coefficient of performance (COP) of the novel thin-film TEC were compared with the traditional design. The results provided a useful guide for the design of the thin-film TEC with high cooling performance and better reliability.

2. The mathematical model

2.1. The physical model

The schematic diagrams of the novel and traditional thin-film TEC are presented in Figure 1. The traditional thin-film TEC consists of 8 pairs of n-type and p-type thermoelements assembled electrically in series and thermally in parallel, while the novel thin-film TEC consists of 4 pairs of coupled-thermoelements assembled electrically in series and thermally in parallel, every coupled-thermoelements consists of two thermoelements made by the same n-type and p-type thermoelectric material. The overall size of the thin-film TEC is $1400 \times 1400 \times 34$ μm^3. The Bi_2Te_3-based thin-film thermoelectric material is used for the thermoelement. The thickness of the thermoelements is 20 μm and the thermoelements are located between the top and bottom copper slices with a thickness of 2 μm. The cross-sectional area of the thermoelements is 200×200 μm^2. Aluminum oxide (Al_2O_3) with a thickness of 2 μm is used as the ceramic plates. The critical parameters of the novel and traditional thin-film TEC are summarized and listed in Table 1. The temperature independent properties of copper and aluminum oxide are adopted from the material library of the ANSYS software, and the temperature dependent thermo-mechanical properties of Bi_2Te_3 are incorporated into the analysis, as listed in Table 2.

Table 1. Basic parameters of the thin-film TEC.

The parameters	Dimensions
Thermoelement length (μm)	20
Copper slices thickness (μm)	5
Ceramic plate thickness (μm)	2
Thermoelement gap distance (μm)	200
Cross-sectional area of the thermoelement (μm^2)	200×200

Table 2. Material properties used for the modeling [33, 34, 35].

Material	Material properties	Material properties
p-Bi_2Te_3	Thermal conductivity ($W/(m \cdot K)$)	$13.04 - 0.14T + 5.81 \times 10^{-4}T^2 - 1.03 \times 10^{-6}T^3 + 6.62 \times 10^{-5}T^4$
	Electrical resistivity ($\Omega \cdot m$)	$3.94 \times 10^{-5} - 3.12 \times 10^{-7}T + 9.52 \times 10^{-10}T^2 - 8.07 \times 10^{-13}T^3$
	Seebeck coefficient (V/K)	$2.71 \times 10^{-3} - 2.58 \times 10^{-5}T + 9.59 \times 10^{-8}T^2 - 1.51 \times 10^{-10}T^3 + 8.53 \times 10^{-14}T^4$
n-Bi_2Te_3	Thermal conductivity ($W/(m \cdot K)$)	$-1.27 + 0.02T - 3.41 \times 10^{-5}T^2 + 2.18 \times 10^{-8}T^3 - 1.55 \times 10^{-15}T^4$
	Electrical resistivity ($\Omega \cdot m$)	$5.40 \times 10^{-5} - 3.40 \times 10^{-7}T + 8.29 \times 10^{-10}T^2 - 6.06 \times 10^{-13}T^3$
	Seebeck coefficient (V/K)	$4.29 \times 10^{-5} - 9.75 \times 10^{-7}T + 9.56 \times 10^{-10}T^2 + 1.39 \times 10^{-13}T^3$
Cu	Thermal conductivity ($W/(m \cdot K)$)	398
	Electrical resistivity ($\Omega \cdot m$)	1.8×10^{-7}
Al_2O_3	Thermal conductivity ($W/(m \cdot K)$)	37.2

2.2. The layout forms of the disabled thermoelements

The reliability of thermoelectric module is a vital factor for the thermoelectric application, particularly for the thin-film TEC whose thermoelements are very small and fragile. We proposed a novel thin-film TEC with a couple of thermoelements electrically connected in parallel and then electrically connected in series to other coupled-thermoelements. To exhibit the superiority of the novel thin-film TEC in reliability, we compare the cooling performance of the novel thin-film TEC with the traditional one whose thermoelements are connected electrically in series. Under normal circumstances, there are 16 thermoelements in both the novel and the traditional thin-film TEC. However, several thermoelements may malfunction so that the thin-film TEC will work inefficiently. In this paper, 2 and 4 thermoelements, respectively, are set to be disabled to figure out the reliability of the novel and the traditional thin-film TECs. For the novel thin-film TEC, the 2 and 4 disabled thermoelements can be arranged in two forms. As shown in Figure 2, the color of the disabled thermoelements were set to be purple. For Form #1, the broken thermoelements are connected electrically in series among different coupled-thermoelements. While for Form #2, the 2 disabled thermoelements are

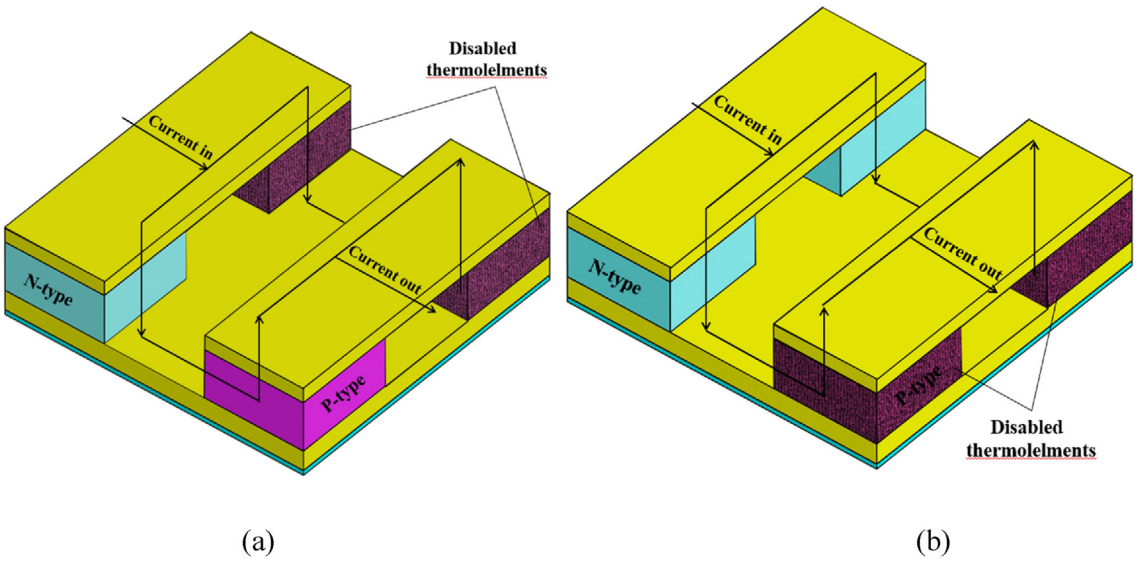

Figure 2. The layout of the disabled thermoelements: (a) Form #1; (b) Form #2.

connected electrically in parallel within one coupled-thermoelements. Usually, Form #1 is more possible to happen than Form #2. For the traditional thin-film TEC, all the disabled thermoelements are electrically connected in series. We studied the reliability by comparing the maximum cooling capacity ($Q_{c,max}$), the maximum cooling temperature (ΔT_{max}), and the coefficient of performance (COP) for both novel and traditional thin-film TECs.

2.3. Governing equations

The three-dimensional governing equations that couple the temperature T and electrical current density $\vec{j}$ are given by [5, 36].

$$\nabla \cdot (k\nabla T) + \gamma \vec{j}^{2} - T\frac{\partial \alpha}{\partial T}\vec{j} \cdot \nabla T = 0 \tag{1}$$

$$\vec{j} = \frac{1}{\rho}\left(\vec{E} - \alpha \nabla T\right) \tag{2}$$

where k, γ, and α represent the thermal conductivity, electrical resistivity, and Seebeck coefficient, respectively, and they are all functions of temperature. $\vec{E}$ is the electric field intensity vector. And ∇T indicates the temperature gradient.

The first term of Eq. (1) represents the Fourier heat conduction, the second term refers to the Joule heat that exists in all current carrying materials, and the third term represents the Thomson heat when the Seebeck coefficient depends on temperature.

When delivering the current I to the thin-film TEC, the heat absorbed Q_c at the cold-end and heat released Q_h at the hot-end can be calculated by [37] Eqs. (3) and (4).

$$Q_c = \alpha_{pn} I T_c - \frac{I^2 R}{2} - K\,(T_h - T_c) \tag{3}$$

$$Q_h = \alpha_{pn} I T_h + \frac{I^2 R}{2} - K(T_h - T_c) \tag{4}$$

where T_h, and T_c are hot-end and cold-end temperature of the TEC, respectively. R indicates the total electrical resistance, including the electrical contact resistance and the material electrical resistance. And the α_{pn} is the sum of the Seebeck coefficients of p-type and n-type thermoelements. The first, the second, and the third term in Eqs. (3) and (4) are the Peltier heat, Joule heat, and Fourier heat, respectively. While Peltier effect is reversible, Joule heating and Fourier heat conduction are irreversible.

The three key indicators, maximum cooling capacity ($Q_{c,max}$), maximum cooling temperature (ΔT_{max}), and the coefficient of performance (COP), are often used to evaluate the cooling performance of the thin-film TEC, which are calculated by Eqs. (5), (6), (7), (8), and (9). The cooling capacity can reach the maximum value when $T_h = T_c$, in this condition, Eq. (3) is reduced to

$$Q_{c,max} = \alpha_{pn} I T_c - \frac{I^2 R}{2} \tag{5}$$

The temperature difference (ΔT) built in the TEC is

$$\Delta T = T_h - T_c \tag{6}$$

Let $\frac{dQ_c}{dI} = 0$, the current (I_{max}) for the maximum cooling capacity [38] is given by

$$I_{max} = \frac{\alpha_{pn} T_c}{R} \tag{7}$$

The thin-film TEC achieves the maximum cooling temperature (ΔT_{max}) when the heat load at cold side equals zero ($Q_c = 0$), the ΔT_{max} can be calculated by [39].

$$\Delta T_{max} = (T_h - T_c)_{max} = \frac{1}{2} Z T_c^2 \tag{8}$$

The COP acquired by Q_h and Q_c is given by:

$$COP = \frac{Q_c}{Q_h - Q_c} = \frac{\alpha_{pn} I T_c - \frac{I^2 R}{2} - K\,(T_h - T_c)}{\alpha_{pn} I (T_h - T_c) + I^2 R} \tag{9}$$

2.4. The boundary conditions

The following assumptions were introduced to simplify the modeling. These assumptions were thought had negligible influence on the final results.

(a) The thermophysical properties of the ceramic plates and copper slices were assumed to be independent of temperature.
(b) Electrical and thermal contact resistances were considered at the interface between the thermoelement and the copper slices. The electrical contact resistance increased substantially when a thermoelement didn't function well.

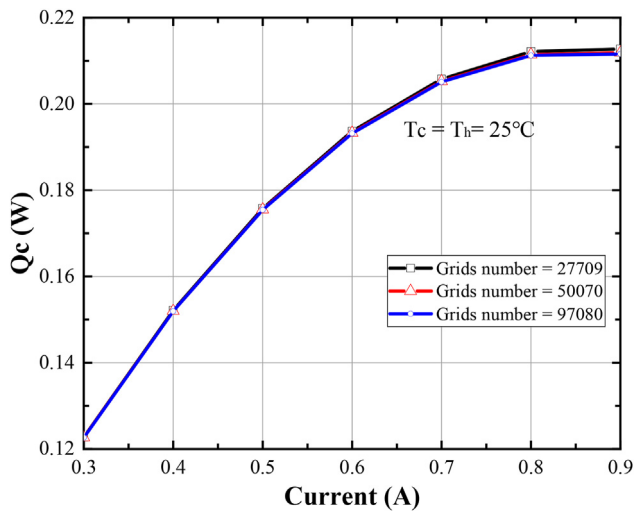

Figure 3. Comparison of the cooling capacity profiles with three different grid systems.

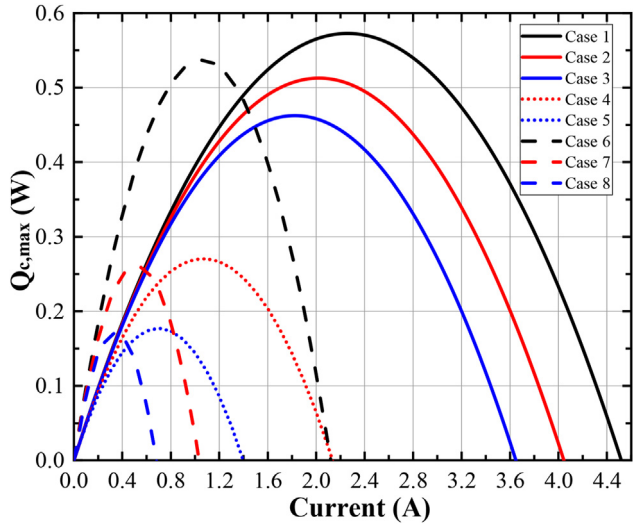

Figure 4. $Q_{c,max}$ variations of the novel and the traditional thin-film TEC with different electrical current.

(c) All the surfaces except the cold and the hot-ends of the thin-film TEC were assumed to be thermally insulated.

To calculate the $Q_{c,max}$ and COP, the initial temperatures of the cold-end and the hot-end were both maintained at 25 °C. To calculate the ΔT_{max}, the initial temperature of the hot-end was maintained at 25 °C, while the cold-end was considered to be thermal isolated. The ambient temperature was set as 25 °C. In this work, we defined the thermal contact resistance of mental-semiconductor interface as 8×10^{-8} $K{\cdot}m^2{\cdot}W^{-1}$, a theoretical limit predicted by Chen [25]. The electrical contact resistivity between the copper slice and Bi_2Te_3-based thermoelectric materials was set as 10^{-7} $\Omega{\cdot}cm^2$ [40,41]. And the electrical contact resistivity was assumed increased to 10^{-3} $\Omega{\cdot}cm^2$ when the corresponding thermoelement was broken [40, 42].

2.5. Model validation

The temperature and electrical governing equations (Eqs. (1) and (2)) were solved by ANSYS Workbench 19.0 based on the finite element method. In order to verify the grid independence of the simulations, three different grid systems with total elements of 27709, 50070, and 97080 were examined at same boundary condition, as shown in Figure 3. The simulations were carried out based on the novel thin-film TEC with 16 thermoelements. Different currents were applied to the novel thin-film TEC to compare the $Q_{c,max}$ for the three grid systems. As shown in Figure 2, the $Q_{c,max}$ of three different grid systems were almost identical when the current was less than 0.5 A, and the distinction for the three cases was minimum when the current was larger than 0.5 A. It can be concluded that the numerical results were grid-independent. To save the computational cost, a grid number of 27709 was chosen to perform the analysis.

3. Results and discussion

3.1. The comparisons of $Q_{c,max}$

As shown in Figure 4, with the increasing of electrical current, the $Q_{c,max}$ increases to the peak value firstly and then decreases to zero for both the novel and the traditional thin-film TECs. This is because that the Peltier effect which contributes to increasing the cooling capacity plays a primary role when the electrical current is small, while the Joule heat which offsets the cooling effect makes a difference when the electrical current is larger than the optimal electrical current (I_{opt}). In addition, the $Q_{c,max}$ and the optimal electrical currents decrease as the number of thermoelement that works normally decreases. This attributes to the increasing electrical resistance caused by the disabled thermoelements.

When all the 16 thermoelements work normally, the $Q_{c,max}$ of the novel thin-film TEC is 0.57 W with I_{opt} = 2.25A, and $Q_{c,max}$ of the traditional thin-film TEC is 0.54 W with I_{opt} = 1.05 A. The former $Q_{c,max}$ is almost equal to the latter one, due to the same geometry of the thermoelement. However, the I_{opt} of the novel thin-film TEC is 2.14 times that of the traditional thin-film TEC, which is mainly resulted by two factors: first, only half of the electrical current passes through every thermoelement in the novel thin-film TEC; second, the total electrical resistance of the novel thin-film TEC model is smaller than that of the traditional thin-film model due to the larger cross-sectional area of the copper slice.

For the novel thin-film TEC, the disabled thermoelements are arranged in Forms #1, the I_{opt} for case 2 and case 3 are 2.05 A and 1.85 A, respectively. And the $Q_{c,max}$ for case 2 and case 3 are 0.51W and 0.46W, respectively. The decline rates of the $Q_{c,max}$ among case 1, case 2, and case 3 are 11.8% and 32.6%, respectively. For the novel thin-film TEC that disabled thermoelements are arranged in Forms #2, the I_{opt} for case 4 and case 5 are 1.10 A and 0.70 A, respectively. And the $Q_{c,max}$ for case 4 and case 5 are 0.27 W and 0.18 W, respectively. The decline rates of the

Table 3. The detail data of $Q_{c,max}$ for the novel and the traditional thin-film TECs.

Case	Novel thin-film TEC						Traditional thin-film TEC		
	Form #1			Form #2					
	1	2	3	1	4	5	6	7	8
Number of thermo-element working normally	16	14	12	16	14	12	16	14	12
I_{opt} (A)	2.25	2.05	1.85	2.25	1.10	0.70	1.05	0.50	0.30
$Q_{c,max}$ (W)	0.57	0.51	0.46	0.57	0.27	0.18	0.54	0.26	0.17
Decline rate of $Q_{c,max}$	11.8%	32.6%		111.1%	50.0%		107.7%	52.96%	

$Q_{c,max}$ among case 1, case 4, and case 5 are 111.1% and 50.0%. For the traditional thin-film TEC, the I_{opt} for case 7 and case 8 are 0.50 A and 0.30 A, respectively. And the $Q_{c,max}$ are 0.26 W and 0.17 W, respectively. The decline rates of $Q_{c,max}$ among case 6, case 7 and case 8 are 107.7% and 52.96%. The detail performance date of the novel and the traditional thin-film TECs is also listed in Table 3.

For Form #1, with more disabled thermoelements, the $Q_{c,max}$ for the novel thin-film TEC is much larger than that of the traditional design. For example, the $Q_{c,max}$ for the novel thin-film TEC is 1.96 times as that for the traditional thin-film TEC when 14 thermoelements work normally. However, decline rate of the $Q_{c,max}$ for the traditional thin-film TEC is 1.62–9.12 times as that for the novel thin-film TEC. It shows that, when disabled thermoelements are arranged in Form #1, the traditional TEC is more sensitive to the broken thermoelements. However, for Form #2, the $Q_{c,max}$ for both the novel and the traditional thin-film TECs are influenced significantly by the broken thermoelements.

3.2. The comparison of COP

Figure 5 shows the COP variations of the novel and the traditional thin-film TEC with different current. The COP is calculated from the $Q_{c,max}$ in Section 3.1. It was found that the COP of the novel and the traditional thin-film TECs reduces monotonously with the electric current increasing. In addition, the more disabled thermoelements, the smaller COP. It is clear that the COP of the novel thin-film TEC is much higher than that of the traditional design. For example, when 16 thermoelements that work efficiently, the COP is 4.01 and 1.62 at the current of 0.5A for the novel thin-film TEC and the traditional thin-film TEC, respectively. The COP of the former is 2.48 times as that of the latter, which indicates that the novel thin-film TEC has a better cooling efficiency. For 14 thermoelements that work normally, the COP of case 2, case 4, and case 7 are 3.55, 1.64, and 0.54 at the current of 0.5A, respectively. Compared with 16 thermoelements that work normally, it can be seen that the COP decreases as the number of thermoelement that works normally decreases. The decline rate of the COP among case 1 and case 2, case 1 and case 4, case 6 and case 7 are 12.9%, 301% and 200%, respectively. The decline rate of the novel thin-film TEC for Form #1 is the smallest, which indicates that the novel thin-film TEC for Form #1 has the superior reliability.

3.3. The comparison of ΔT_{max}

In this part, to get the maximum temperature difference (ΔT_{max}), the interface of the cold-end is set to be adiabatic, and the temperature of the hot-end is assumed to be 25 °C. Thus, the ΔT_{max} can be calculated by (25-T_c). Figure 6 depicts the ΔT_{max} variations of the novel thin-film TEC and the traditional thin-film TEC with different electrical current. The ΔT_{max} increases with the electrical current firstly but then decreases after it met its maximum value at the I_{opt}. The I_{opt} of ΔT_{max} are identical to I_{opt} of the $Q_{c,max}$ in Section 3.1, which indicates that the $Q_{c,max}$ and the ΔT_{max} occur at the same condition.

When all the 16 thermoelements work normally, it is observed that the ΔT_{max} of the novel and the traditional thin-film TEC are 10.45 °C and 8.67 °C, respectively. Similar as the COP of the novel and the traditional thin-film TEC in Section 3.2, the ΔT_{max} of the novel thin-film TEC is higher than that of the traditional thin-film TEC. Therefore it can be concluded that the novel thin-film TEC has a better cooling capability than the traditional thin-film TEC. As the number of thermoelements that work efficiently decreases, ΔT_{max} decreases as well. For example, the ΔT_{max} of the case 2, case 4, and case 7 are 9.36 °C, 5.36 °C, and 4.95 °C for 14 thermoelements that work efficiently, respectively.

For the novel thin-film TEC, the disabled thermoelements are arranged in Form #1, the ΔT_{max} for case 2 and case 3 are 9.36 °C and 8.48 °C, respectively. The decline rate of the ΔT_{max} among case 1, case 2, and case 3 are 11.2% and 10.34%. For the novel thin-film TEC that disabled thermoelements are arranged in Form #2, the ΔT_{max} for case 4 and case 5 are 5.36 °C and 3.42 °C, respectively. The decline rate of the ΔT_{max} among case 1, case 4, and case 5 are 94.2% and 56.7%. For the traditional thin-film TEC, the ΔT_{max} are 4.95 °C and 3.39 °C, respectively. The decline rate of $Q_{c,max}$ among case 6, case 7 and case 8 are 75.2% and 46.0%. The detail date of $Q_{c,max}$ for the novel and the traditional thin-film TECs is listed in Table 4.

For Form #1, with more disabled thermoelements, the ΔT_{max} for the novel thin-film TEC is much larger than that of the traditional design. For example, the ΔT_{max} for the novel thin-film TEC is 1.89 times as that for the traditional thin-film TEC when 14 thermoelements work normally. However, decline rate of the ΔT_{max} for the traditional thin-film TEC is 4.45–8.41 times as that for the novel thin-film TEC. It shows that, when disabled thermoelements are arranged in Form #1, the traditional TEC is more sensitive to the broken thermoelements. However, for Form #2, the ΔT_{max} for both the novel and the traditional thin-film TEC are influenced significantly by the broken thermoelements. It is obvious that the novel thin-film TEC for Form #1 is superior to others in ΔT_{max} and reliability.

3.4. The comparison of Q_c under different ΔT

In this part, the Q_c of the novel and the traditional thin-film TECs is compared, as shown in Figure 7. The temperature of the cold-end is fixed

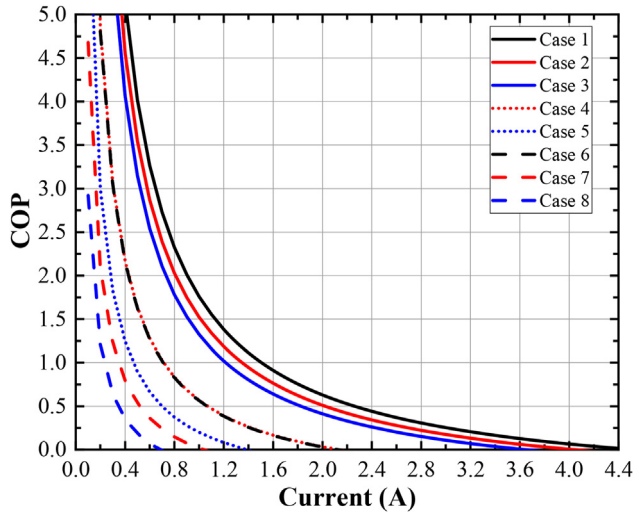

Figure 5. COP variations of the novel and the traditional thin-film TEC with different electrical current.

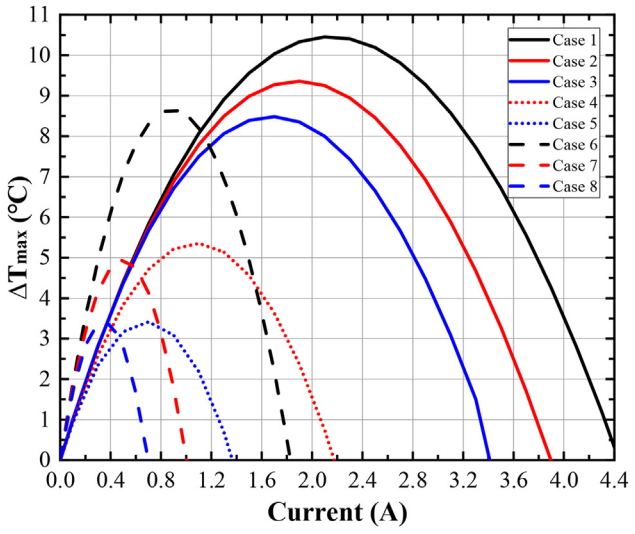

Figure 6. ΔT_{max} variations of the novel and the traditional thin-film TEC with different electrical current.

Table 4. The detail date of $Q_{c,max}$ for the novel and the traditional thin-film TECs.

Case	Novel thin-film TEC						Traditional thin-film TEC		
	Form #1			Form #2					
	1	2	3	1	4	5	6	7	8
ΔT_{max} °C	10.41	9.36	8.48	10.41	5.36	3.42	8.67	4.95	3.39
Decline rate of ΔT_{max}	11.2%	10.34%		94.2%	56.7%		75.2%	46.0%	

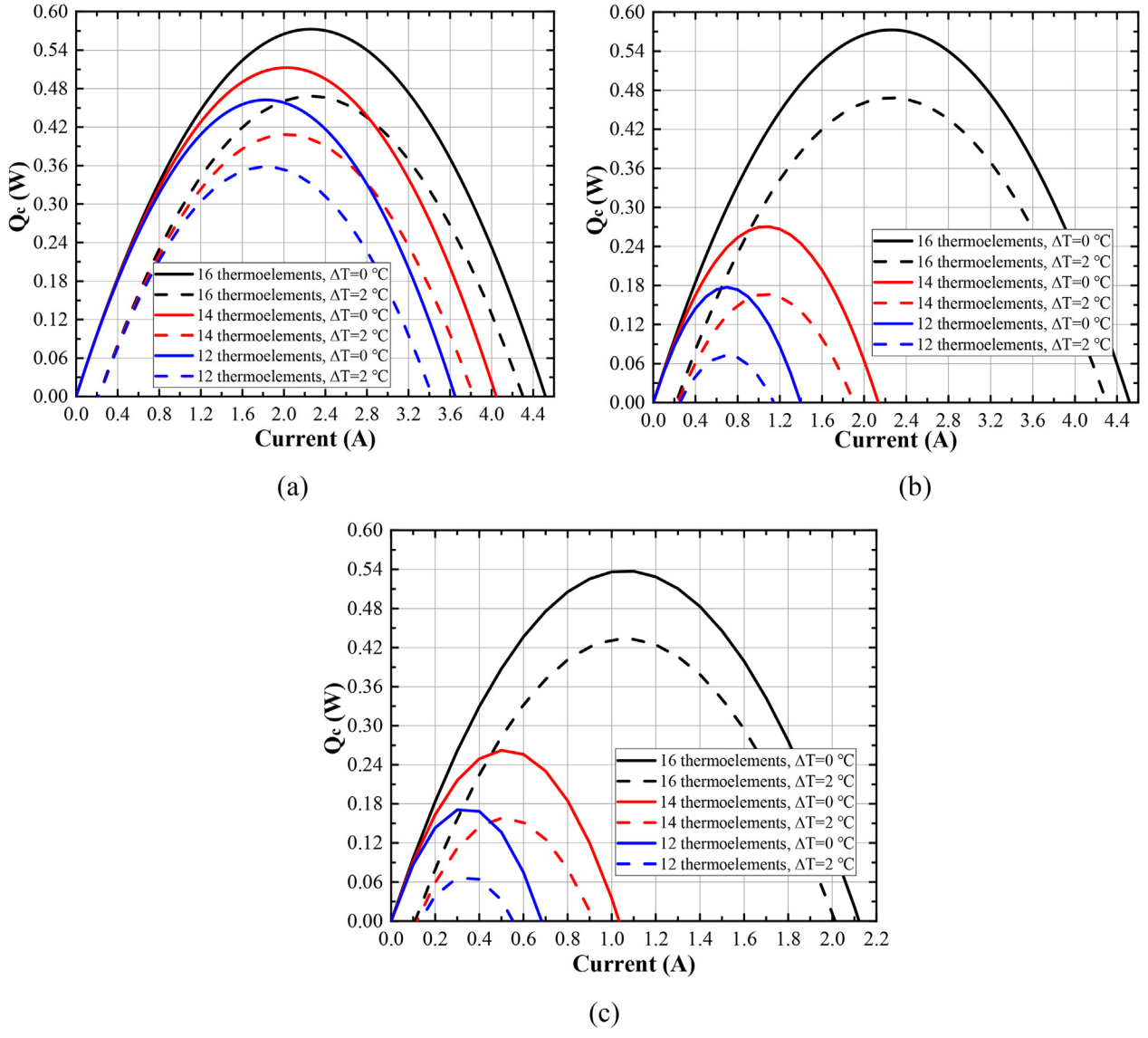

Figure 7. . Q_c variations of the thin-film TEC under different ΔT: (a) the novel thin-film TEC that disabled thermoelements are arranged in Form #1 and (b) Form #2; (c) the traditional thin-film TEC.

to $T_c = 25$ °C, and the difference between the hot-end and the cold-end is assumed to be $\Delta T = 0$ °C and $\Delta T = 2$ °C, respectively. Figure 7 (a) shows the Q_c of the novel thin-film TEC that disabled thermoelements are arranged in Form #1. It can be found that Q_c increases with the increase of the at first and reaches a maximum value, then the Q_c decreases with the increase of electrical current. This trend is same as the $Q_{c,max}$ in Section 3.1. And the Q_c decrease as the number of thermoelements that operate normally decreases. Moreover, the Q_c is reduced as ΔT is increased from 0 °C to 2 °C. For example, when 14 thermoelements that work normally, the Q_c of the novel thin-film TEC are 0.51 W and 0.41 W at the ΔT of 0 °C and 2 °C, respectively. This happens because that the Fourier's heat that conducts from the hot-end to the cold-end of the thin-film TEC eliminates the cooling capacity of the Peltier effect. Figure 7 (b) shows the Q_c of the novel thin-film TEC that disabled thermoelements are arranged in Form #2. When 14 thermoelements that work efficiently, the maximum Q_c of the novel thin-film TEC are 0.27 W and 0.17 W at the ΔT of 0 °C and 2 °C, respectively. The reduction of the Q_c of 0.1W is same as the reduction in Figure 6 (a). The difference from Figure 7 (a) is that the Q_c decreases greatly as the number of thermoelements that operate efficiently decreases. Figure 7 (c) shows the Q_c of the traditional thin-film TEC. The curves in Figure 7 (c) are very similar to those in Figure 7 (b), which indicates that the performance of the novel thin-film TEC that disabled

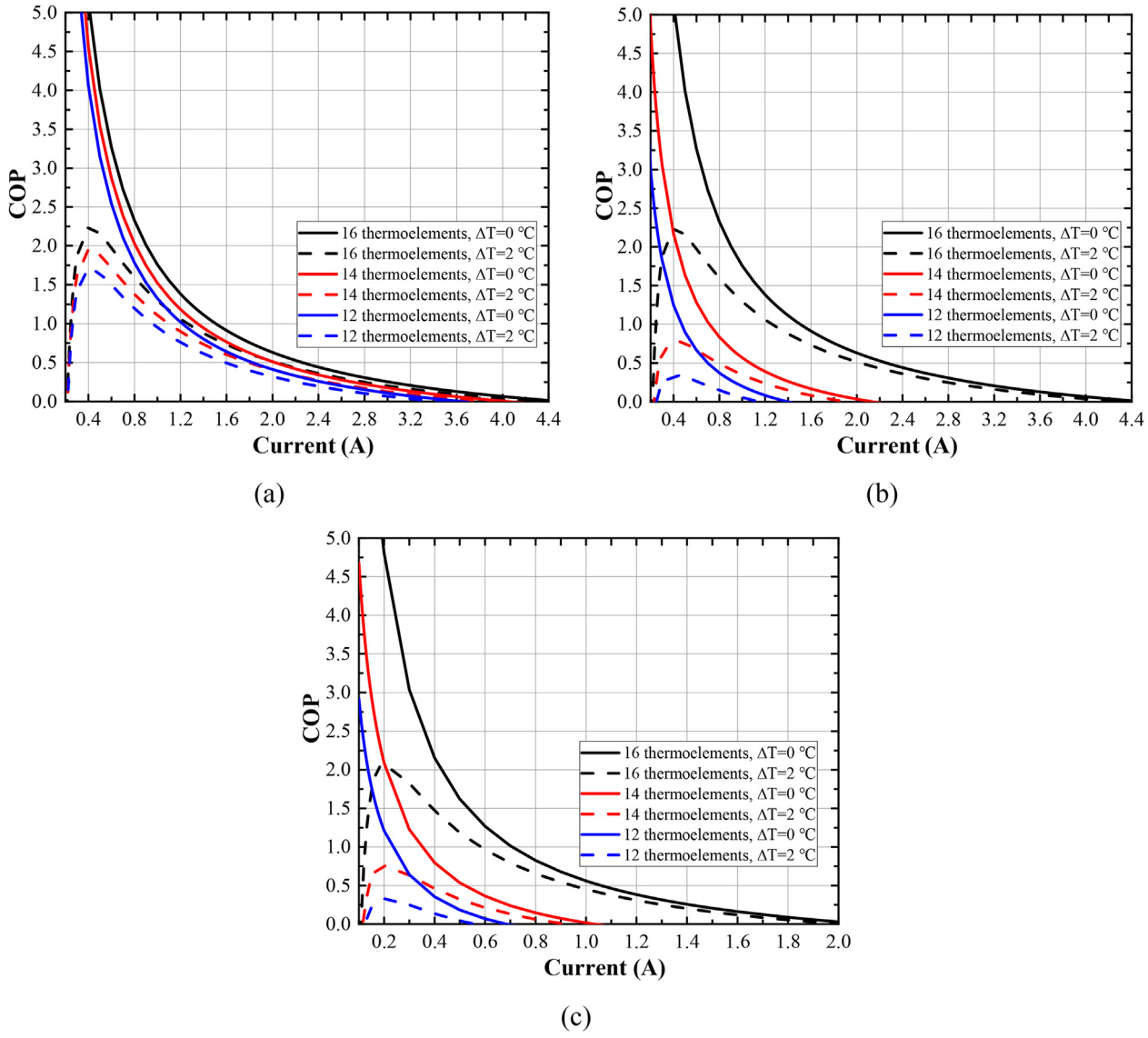

Figure 8. COP variations with current of the thin-film TEC for $\Delta T = 0$ °C or $\Delta T = 2$ °C: the novel thin-film TEC in which disabled thermoelements are arranged in (a) Form #1 and (b) Form #2; (c) the traditional thin-film TEC.

thermoelements are arranged in Form #2 is uniform with the traditional thin-film TEC.

3.5. The comparison of COP under different ΔT

Figure 8 shows the COP variations of the novel and the traditional thin-film TECs under different ΔT. Figure 8 (a) shows the COP variations of the novel thin-film TEC in which the disabled thermoelements are arranged in Form #1 under different ΔT. When $\Delta T = 0$ °C, the COP decreases monotonously with the electric current increasing. When $\Delta T = 2$ °C, the COP increases to the peak value of 2.25 at an electrical current of 0.4 A, and then decreases to 0 gradually. The COP for $\Delta T = 2$ °C is always smaller than the COP for $\Delta T = 0$ °C. The larger ΔT resulted in the lower COP. When $\Delta T = 2$ °C, The maximum COPs of the novel thin-film TECs with 16, 14, and 12 normal thermoelements are 2.24, 1.96, and 1.65, respectively. The decline rates of COP are 12.3% and 18.8% between every two cases. Figure 8 (b) shows the COP variations of the novel thin-film TEC in which the disabled thermoelements are arranged in Form #2 under different ΔT. The COP decreases more significantly for both $\Delta T = 0$ °C and $\Delta T = 2$ °C. For example, when $\Delta T = 2$ °C, the maximum COP of the novel thin-film TEC with 16, 14, and 12 normal thermoelements are 2.24, 0.80, and 0.35, respectively. The decline rates of COP are 180% and 56.3% between every two cases. Furthermore, the maximum COP appears at the same electrical current of 0.4 A as Figure 8 (a). Figure 8 (c) shows the COP variations of the traditional thin-film TEC under different ΔT. The trend of the variations is same as that in Figure 8 (b). While the maximum COP appears at the electrical current of 0.2 A, which is a half of the optimal electrical current in Figure 8 (a) and (b). This is caused by the parallel coupled-thermoelements where only half of the electrical current passes through every thermoelement in the novel thin-film TEC.

4. Conclusion

In summary, we proposed a novel thin-film TEC with a couple of thermoelements electrically connected in parallel and then electrically connected in series to the next couple of thermoelements. The cooling performance of novel thin-film TEC was compared with the traditional design. The maximum cooling capacity, the maximum cooling temperature, and the coefficient of performance of the novel and the traditional thin-film TEC were systematically studied in case several thermoelements in the TEC were broken. The conclusions could be drawn from the results as follows:

(1) The optimal electrical current of the novel thin-film TEC was 2.14 times of that for the traditional thin-film TEC due to the parallel connection of the thermoelements.
(2) When all the thermoelements work normally, the maximum cooling capacity, the maximum cooling temperature and the coefficient of performance of the novel thin-film TEC were larger than the traditional thin-film TEC.
(3) When several thermoelements cracked, the maximum cooling capacity, the maximum cooling temperature, and the coefficient of performance of the traditional thin-film TEC decreased sharply. Meanwhile, the novel thin-film TEC was insensitive to the local cracks.
(4) The reliability of the novel thin-film TEC where the broken thermoelements arranged in Form #1 is significantly better than Form #2 and the traditional thin-film TEC. Form #2 was unlike to happen in real device.

The design of the novel thin-film TEC made a reference for the enhancement of cooling performance and reliability of the thin-film TEC. Experimental validation was undertaking in the lab to validate the modeling results.

Declarations

Author contribution statement

Tingzhen Ming, Yongjia Wu: Conceived and designed the experiments; Wrote the paper.

Sen Chen: Performed the experiments; Wrote the paper.

Yonggao Yan, Jianlong Wan: Analyzed and interpreted the data.

Tingrui Gong: Contributed reagents, materials, analysis tools or data.

Funding statement

This work was supported by the National Key Research and Development Plan (Key Special Project of Inter-governmental National Scientific and Technological Innovation Cooperation, Grant No. 2019YFE0197500), the European Commission H2020 Marie Curie Research and Innovation Staff Exchange (RISE) award (Grant No. 871998), Key Research and Development Projects of Hubei Province (Grant No. 2020BAB129), and the Scientific Research Foundation of Wuhan University of Technology (Grant Nos. 40120237 and 40120551), and the Fundamental Research Funds for the Central Universities (Grant No. WUT: 2021IVA037).

Data availability statement

No data was used for the research described in the article.

Declaration of interests statement

The authors declare the following conflict of interest: Tingzhen Ming is part of the Editorial Board for Heliyon Energy & Engineering.

Additional information

No additional information is available for this paper.

Acknowledgements

This research was supported by the Key Research and Development Projects of Hubei Province (Grant No. 2020BAB129), and the Scientific Research Foundation of Wuhan University of Technology (Grant Nos. 40120237 and 40120551), and the Fundamental Research Funds for the Central Universities (Grant No. WUT: 2021IVA037).

References

[1] T. Wang, H. Wu, D. Gao, K. Zhang, J. Meng, Achieving better super-cooling in a two-stage transient thermoelectric device with constraint-free pulse current by multi-objective optimization, J. Therm. Sci. 30 (2021) 1349–1362.
[2] T. Gong, L. Gao, Y. Wu, H. Tan, F. Qin, X. Xin, L. Shen, J. Li, T. Ming, A model to evaluate the device-level performance of thermoelectric cooler with Thomson effect considered, J. Therm. Sci. (2022) 1–15.
[3] T. Pan, T. Gong, W. Yang, Y. Wu, Numerical study on the thermal stress and its formation mechanism of a thermoelectric device, J. Therm. Sci. 27 (2018) 249–258.
[4] W.Z.L. Shen, G. Liu, Z. Tu, Q. Lu, H. Chen, Q. Huang, Performance enhancement investigation of thermoelectric cooler with segmented configuration - ScienceDirect, Appl. Therm. Eng. 168 (2020).
[5] D.M. Rowe, Thermoelectrics Handbook : Macro to Nano, 2005.
[6] O. Owoyele, S. Ferguson, B.T. O'Connor, Performance analysis of a thermoelectric cooler with a corrugated architecture, Appl. Energy 147 (2015) 184–191.
[7] F. Jiang, F. Meng, L.g. Chen, Z. Chen, Thermodynamic analysis and experimental research of water-cooled small space thermoelectric air-conditioner, J. Therm. Sci. 31 (2022) 390–406.
[8] S.B. Riffat, X. Ma, Improving the coefficient of performance of thermoelectric cooling systems: a review, Int. J. Energy Res. 28 (2010) 753–768.
[9] T.C. Harman, P.J. Taylor, M.P. Walsh, B.E. Laforge, Self-assembled Quantum Dot Superlattice Thermoelectric Materials and Devices, 2004.
[10] G. Min, D.M. Rowe, Improved model for calculating the coefficient of performance of a Peltier module, Energy Convers. Manag. 41 (2000) 163–171.
[11] H.L. Kong, O.J. Kim, Analysis on the cooling performance of the thermoelectric micro-cooler, Int. J. Heat Mass Tran. 50 (2007) 1982–1992.
[12] L.S.D. Sun, H. Chen, B. Jiang, D. Jie, H. Liu, J. Tang, Modeling and analysis of the influence of Thomson effect on micro-thermoelectric coolers considering interfacial and size effects, Energy 196 (2020).
[13] X. Zhou, Y. Yan, X. Lu, H. Zhu, X. Han, G. Chen, Z. Ren, Routes for high-performance thermoelectric materials, Mater. Today (2018) 974–988. S1369702118300907.
[14] G. Min, D.M. Rowe, "Symbiotic" application of thermoelectric conversion for fluid preheating/power generation, Energy Convers. Manag. 43 (2002) 221–228.
[15] L.G.T. Gong, Y. Wu, L. Zhang, S. Yin, J. Li, T. Ming, Numerical simulation on a compact thermoelectric cooler for the optimized design - ScienceDirect, Appl. Therm. Eng. 146 (2019) 815–825.
[16] H.J.X. Nie, X. Sang, P. Wei, W. Zhu, W. Zhao, Q. hang, Numerical simulation and structural optimization of multi-stage planar thermoelectric coolers, Phys. Status Solidi (2020) 217.
[17] A.J. Gross, G.S. Hwang, B. Huang, H. Yang, N. Ghafouri, H. Kim, R.L. Peterson, C. Uher, M. Kaviany, K. Najafi, Multistage planar thermoelectric microcoolers, J. Microelectromech. Syst. 20 (2011) 1201–1210.
[18] M.S. Shamim, R.S. Narde, J.L. Gonzalez-Hernandez, A. Ganguly, J. Venkatarman, S.G. Kandlikar, Evaluation of wireless network-on-chip architectures with microchannel-based cooling in 3D multicore chips, Sustain. Comput.: Inf. Syst. 21 (2019) 165–178.
[19] B.Y.P. Wang, Cohen. Bar, Mini-contact enhanced thermoelectric coolers for on-chip hot spot cooling, Heat Tran. Eng. 30 (2009) 736–743.
[20] Mahdihassan, 849. Thin film thermoelectrics, Vacuum 15 (1965) 523.
[21] H. Bottner, Micropelt miniaturized thermoelectric devices: small size, high cooling power densities, short response time, in: International Conference on Thermoelectrics, 2005.
[22] G.E. Bulman, E. Siivola, B. Shen, R. Venkatasubramanian, Large external ΔT and cooling power densities in thin-film Bi 2 Te 3 -superlattice thermoelectric cooling devices, Appl. Phys. Lett. 89 (2006) 2141–2146.
[23] V. Semenyuk, Miniature thermoelectric modules with increased cooling power, in: International Conference on Thermoelectrics, 2006.
[24] Y. Yu, W. Zhu, X. Kong, Y. Wang, P. Zhu, Y. Deng, Recent development and application of thin-film thermoelectric cooler, Front. Chem. Sci. Eng. (2019) 492–503.
[25] G. Chen, Nanoscale Energy Transport and Conversion : a Parallel Treatment of Electrons, Molecules, Phonons, and Photons, Nanoscale Energy Transport and Conversion : a Parallel Treatment of Electrons, Molecules, Phonons, and Photons, 2005.
[26] L. Cao, D. Yuan, H. Gao, Y. Wang, X. Chen, Z. Zhu, Towards high refrigeration capability: the controllable structure of hierarchical Bi0.5Sb1.5Te3 flakes on a metal electrode, Phys. Chem. Chem. Phys. 17 (2015).
[27] Thermoelectric coolers for thermal gradient management on chip, in: Asme International Mechanical Engineering Congress & Exposition, 2010.
[28] L. Su, L. Wang, T. Shi, P. Cai, M. Huang, C. Wang, C. Hong, P. Dong, Reliability and Non-hermetic Properties of Ge/Si Optoelectronic Devices, IEEE, 2015.
[29] L.G.T. Gong, Y. Wu, H. Tan, F. Qin, T. Ming, J. Li, Transient thermal stress analysis of a thermoelectric cooler under pulsed thermal loading, Appl. Therm. Eng. 162 (2019), 114240.
[30] C.H. Cheng, S.Y. Huang, Development of a non-uniform-current model for predicting transient thermal behavior of thermoelectric coolers, Appl. Energy 100 (2012) 326–335.
[31] A. Schmitz, C. Stiewe, E. Müller, Preparation of ring-shaped thermoelectric legs from PbTe powders for tubular thermoelectric modules, J. Electron. Mater. 42 (2013) 1702–1706.
[32] M. Gao, D.M. Rowe, Ring-structured thermoelectric module, Semicond. Sci. Technol. 22 (2007) 880–883.

[33] A.S. Al-Merbati, B.S. Yilbas, A.Z. Sahin, Thermodynamics and thermal stress analysis of thermoelectric power generator: influence of pin geometry on device performance, Appl. Therm. Eng. 50 (2013) 683–692.
[34] Y. Wu, T. Ming, X. Li, P. Tao, K. Peng, X. Luo, Numerical simulations on the temperature gradient and thermal stress of a thermoelectric power generator, Energy Convers. Manag. 88 (2014) 915–927.
[35] Y. Shan, K.J. Tseng, J. Zhao, Thermal-mechanical design of sandwich SiC power module with micro-channel cooling, in: IEEE International Conference on Power Electronics & Drive Systems, 2013.
[36] T. Gong, Y. Wu, L. Gao, L. Zhang, J. Li, T. Ming, Thermo-mechanical analysis on a compact thermoelectric cooler, Energy 172 (2019) 1211–1224.
[37] L. Shen, X. Fu, H. Chen, S. Wang, Investigation of a novel thermoelectric radiant air-conditioning system, Energy Build. 59 (2013) 123–132.
[38] M. Dhannoon, Analytical Study of Miniature Thermoelectric Device, 2016.
[39] Y. Su, J. Lu, B. Huang, Free-standing planar thin-film thermoelectric microrefrigerators and the effects of thermal and electrical contact resistances, Int. J. Heat Mass Tran. 117 (2018) 436–446.
[40] G. Bulman, P. Barletta, J. Lewis, N. Baldasaro, M. Manno, A. Bar-Cohen, B. Yang, Superlattice-based thin-film thermoelectric modules with high cooling fluxes, Nat. Commun. 7 (2016), 10302.
[41] X. Kong, Z. Wei, L. Cao, Y. Peng, S. Shen, D. Yuan, Controllable electrical contact resistance between Cu and oriented-Bi2Te3 film via interface tuning, ACS Appl. Mater. Interfaces 9 (2017) 25606–25614.
[42] I. Chowdhury, R. Prasher, K. Lofgreen, G. Chrysler, S. Narasimhan, R. Mahajan, D. Koester, R. Alley, R. Venkatasubramanian, On-chip cooling by superlattice-based thin-film thermoelectrics, Nat. Nanotechnol. 4 (2009) 235–238.